Nano Res (2010) 3: 369–378
DOI 10.1007/s12274-010-1041-1
Research Article

Direct Electrochemistry of Cytochrome *c* at a Hierarchically Nanostructured TiO_2 Quantum Electrode

Li Liu[1], Ning Wang[1] (✉), Xia Cao[2] (✉), and Lin Guo[1] (✉)

[1] School of Chemistry and Environment, Beijing University of Aeronautics and Astronautics, Beijing 100191, China
[2] School of Material Science and Engineering, Jiangsu University of Science and Technology, Jiangsu 212003, China

Received: 18 February 2010 / Revised: 25 March 2010 / Accepted: 26 March 2010

ABSTRACT

Monodisperse TiO_2 nanoparticles and urchin-like hierarchical TiO_2 nanospheres assembled with ultrathin quantum nanowires (about 2 nm) have been synthesized by a simple template-free wet chemical method. The morphology, structure, and crystallinity of the TiO_2 nanomaterials were investigated by field emission scanning electron microscopy (FESEM), X-ray diffraction (XRD), and high resolution transmission electron microscopy (HRTEM). Electrochemical measurements with the hierarchically nanostructured TiO_2 nanospheres as an electrode showed much better reversibility for direct electrochemistry of cytochrome *c* (cyt *c*) and much higher sensitivity than for an electrode composed of the monodisperse TiO_2 nanoparticles. The excellent performance of the hierarchical TiO_2 nanospheres may result from a quantum size effect, and their favorable nanostructure (with the presence of an abundance of both uniform macropores and mesopores), excellent structural stability and high specific surface area. The relative ionic strength had significant effect on the direct electrochemistry. Very high ionic strengths relative to cyt *c* concentration (*I*/*c*) induced a conformational change of cyt *c* on the nanostructure-coated electrode, from the native state to a partially unfolded one in 25 mmol/L phosphate buffer solution (pH 6.8).

KEYWORDS

Hierarchically nanostructured TiO_2, cytochrome *c*, ionic strength, bioelectrochemistry

1. Introduction

Nanoscale materials with suitable biocompatibility and high surface curvature have been widely utilized to investigate electron transfer in biological systems, and have provided both an improved understanding of the in vivo behavior of redox proteins and a sound basis for the development of practical biosensors and bioanalytical systems [1–4]. In recent years, much attention has been paid to three-dimensional (3-D) hierarchical architectures due to their high specific surface areas and excellent structural stability, as well as their outstanding transportation properties in comparison with their low-dimensional counterparts [5–11]. Thus, it is desirable to apply hierarchical nanoarchitectures in the investigation of biological processes, such as electron transfer in biological systems [12, 13].

TiO_2 is a promising material for such studies by virtue of its optical transparency, good biocompatibility, environmental safety and reasonable electrical conductivity [14]. Nano-TiO_2 has been widely used

Address correspondence to N. Wang, wangning@mse.buaa.edu.cn; X. Cao, caoxia@buaa.edu.cn; L. Guo, guolin@buaa.edu.cn

as a promoter for the investigation of the direct electrochemistry of redox proteins, or as a substrate for the preparation of enzyme electrodes or biosensors [15–18]. In these cases, nano-TiO_2 can induce the proteins to adsorb on the nano-sized surface in an effective orientation for electron transfer between protein and electrode. For applications in catalysis or as biosensors, hierarchically structured TiO_2 may have better size-dependent biocompatible properties resulting from quantum size effects and, based on its structural stability, greater potential for incorporation in devices showing excellent sensitivity and rapid response [19–21]. Nevertheless, in contrast to the wide use of low-dimensional nanoparticles and nanowires, reports of such uses of hierarchical TiO_2 nanostructures are rather limited [22].

Cytochrome *c* (cyt *c*) is a basic redox heme protein which plays an important role in the biological respiratory chain. In a mitochondrion, cyt *c* transfers electrons between two inner-membrane-bound proteins, cyt *c* reductase and cyt *c* oxidase, by docking at specific adsorption sites on these redox partners [23]. The large dipole moment and the electrostatic field of these protein partners cause the heme to be guided into the proper orientation for effective electron transfer [24]. The interaction of cyt *c* with the protein partners is strongly ionic strength-dependent and binding of specific anions to cyt *c* affects both electron transfer kinetics and the redox potential [25]. Due to its well-assembled 3-D structure and biocompatible properties, a hierarchical nano-TiO_2-coated electrode is eminently suitable for investigation of the direct electrochemistry of cyt *c* and the ionic strength effect. Understanding the ways in which fluctuations in the orientation and conformation of cyt *c* depend on the ionic strength of electrolytes is necessary in order to elucidate the mechanism of electron transfer in biological systems. In addition, investigation of the changes in orientation and conformation at a critical ionic strength may provide new insight into our understanding of biological processes involving cyt *c*.

Hence, in this work, we first developed a simple solution method to synthesize urchin-like hierarchical TiO_2 nanospheres assembled with ultrathin quantum nanowires, and then investigated the direct electrochemistry of cyt *c* using an electrode coated with the hierarchically nanostructured TiO_2, and also the effect of ionic strength on the direct electrochemistry. In comparison with a monodisperse TiO_2 nanoparticle-coated electrode, the hierarchical TiO_2 nanomaterial-coated electrode displayed better reversibility for direct electrochemistry of cyt *c* and higher sensitivity for detection of cyt *c*. We also found that the relative ionic strength had a significant impact on the direct electrochemistry. By increasing the ionic strength relative to cyt *c* concentration (*I*/*c*) and thereby decreasing the effective charge of cyt *c*, the conformation of cyt *c* was modulated on the hierarchical-TiO_2 electrode from the native state to a partially unfolded one.

2. Experimental section

2.1 Sample synthesis

For the preparation of urchin-like hierarchical TiO_2 nanospheres, 10 mL of $TiCl_4$ (analytical grade) was dissolved in 100 mL of pure iced water under vigorous stirring until a clear solution was obtained and then 5 mL of $NH_3 \cdot H_2O$ (25% *v*/*v*, analytical grade) was introduced under constant magnetic stirring. The mixture was then refluxed for 4 h when a white powder was observed. The product was collected by centrifugation and rinsed six times with pure water and then alcohol. The procedure for the preparation of monodisperse TiO_2 nanoparticles was almost the same as that for the urchin-like TiO_2 nanospheres, except that the water was substituted by ethylene glycol (EG, analytical grade).

2.2 Characterization

X-ray powder diffraction (XRD) patterns were collected on a Rigaku X-ray diffractometer (Rigaku Goniometer PMG-A2, CN2155D2) with Cu Kα radiation (wavelength = 0.15147 nm). Transmission electron microscopy (TEM) and scanning electron microscopy (SEM) images were obtained by employing a JEOL JEM-2100F transmission electron microscope and a Hitachi S4800 cold-field emission scanning electron microscope (CFESEM). UV–vis spectra were recorded with a UV–vis spectrophotometer (GBC Cintra 10e).

2.3 Electrochemical measurements

Electrochemical measurements were performed with a CHI 660C Electrochemical Analyzer (CH Instruments, USA) in a conventional three-electrode cell. Coated glassy carbon (GC) electrodes were used as the working electrodes, a platinum wire as the counter electrode and an aqueous Ag/AgCl electrode as the reference electrode. A GC electrode (3 mm diameter) was sequentially polished with 1.0, 0.3, and 0.05 μm alumina slurries and then washed and ultrasonicated in water and then ethanol for a few minutes. The cleaned GC electrode was dried with a high-purity nitrogen stream. To accomplish the preparation of the coated electrodes, 1 mg of urchin-like hierarchical TiO_2 nanospheres or monodisperse TiO_2 nanoparticles were dispersed into 1 mL ethanol and then sonicated for 1 h until a homogeneous suspension resulted. 10 μL of the suspension of urchin-like nanospheres (Hi-Ns-TiO_2) or nanoparticles (Np-TiO_2) was spread evenly onto the treated GC electrode surface with a syringe. In order to obtain uniform films, the coated electrode was covered with a small beaker and allowed to dry for over 24 h at room temperature. When prepared by using 25 mmol/L phosphate buffer solution (PBS) (pH 6.8) instead of ethanol to disperse the hierarchical TiO_2 nanospheres, the coated electrode is referred to as Hi-Ns-TiO_2 (PBS). All the coated electrodes were washed thoroughly with PBS and stored in PBS at room temperature when not in used. Horse heart muscle cyt *c* was purchased from Acros and was used without purification. The electrolyte was phosphate PBS at pH 6.8 made from analytical grade Na_2HPO_4 and KH_2PO_4.

3. Results and discussion

3.1 Characterization of urchin-like hierarchical TiO_2 nanospheres (Hi-Ns-TiO_2) and monodisperse TiO_2 nanoparticles (Np-TiO_2)

3.1.1 XRD

The XRD patterns of the as-prepared products are shown in Fig. 1. All of the peaks of both samples match well with Bragg reflections of the standard tetragonal anatase structure (space group $I4_1/amd$ (No. 141),

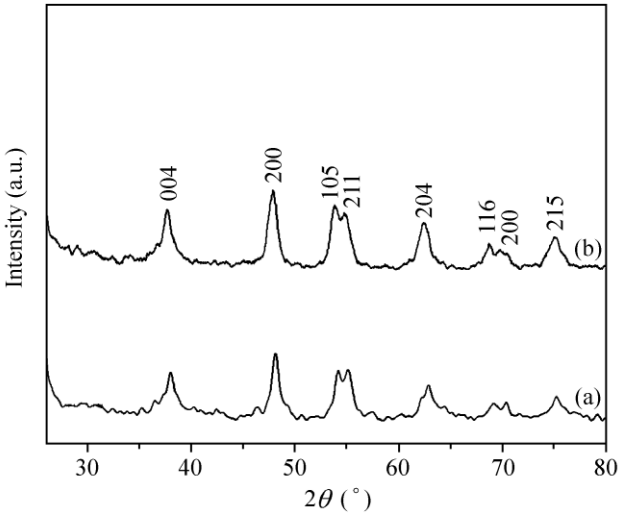

Figure 1 XRD patterns of as-synthesized urchin-like Hi-Ns-TiO_2 (a) and monodisperse Np-TiO_2 (b)

JCPDF # 21-1272). The relatively broad diffraction peaks indicate that the crystals constituting the products are in small in size. The particle sizes were calculated using the Debye–Scherrer formula, $t = 0.89\lambda/(\beta\cos\theta_B)$, where λ is the X-ray wavelength, θ_B is the Bragg diffraction angle, and β is the peak width at half-maximum. The XRD peaks corresponding to the (004) and (200) reflections in Fig. 1 give average particle diameters of 4.2 nm for the nanoparticles and 4.1 nm for the urchin-like nanospheres, indicating that the two materials have the same particle size within experimental error.

3.1.2 SEM and TEM

Figures 2(a) and 2(b) show the SEM images of the as-synthesized anatase TiO_2 nanocrystals. The product synthesized in EG is made up of small TiO_2 nanoparticles with diameter no more than 10 nm (Fig. 2(b)), while the TiO_2 particles synthesized in pure water are urchin-like nanospheres with a hierarchical structure (Fig. 2(a)). Close examination shows that each urchin-like nanosphere, with an average size of about 400–500 nm, is composed of ultrathin nanowires with a diameter of less than 10 nm and a length of up to 200–300 nm. The nanowires tend to aggregate together and form well-dispersed bundles. TEM and high-resolution TEM (HRTEM) were used to study their fine structures (Figs. 2(c) and 2(d)). With a much higher magnification, as revealed by Fig. 2(c), the urchin-like

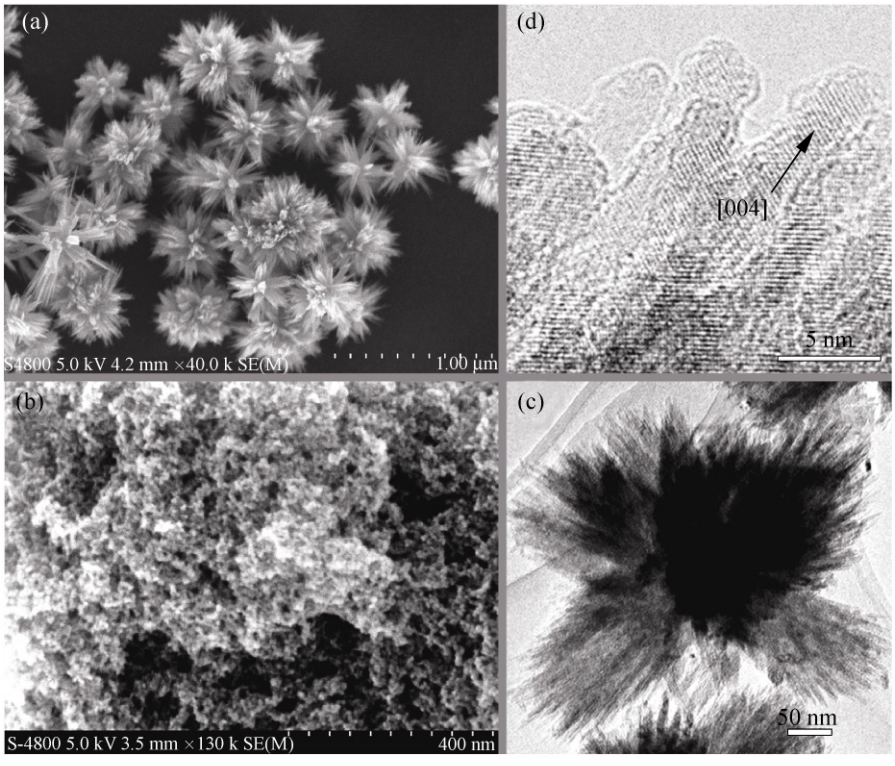

Figure 2 Images of as-synthesized TiO_2 nanomaterials: SEM images of the urchin-like Hi-Ns-TiO_2 (a), monodisperse Np-TiO_2 (b); TEM (c) and HRTEM (d) images of urchin-like Hi-Ns-TiO_2

TiO_2 can be seen to be composed of nanowires with a diameter about 2 nm. An HRTEM image taken from one dispersed nanowire reveals their accurate size, showing that the diameter of the quantum nanowire is about 2.5 nm (Fig. 2(d)). HRTEM images also enabled the viewing of grain boundaries and lattice fringes. As shown in Fig. 2(d), the lattice fringe spacing is measured to be 0.238 nm, which matches well with the d(004) spacing for the anatase TiO_2 tetragonal structure, and is in good agreement with the XRD pattern.

3.2 Electrochemical impedance characterization of urchin-like Hi-Ns-TiO_2-coated electrode and monodisperse Np-TiO_2-coated electrode

Electrochemical impedance spectroscopy (EIS) can provide useful information about the impedance changes of the electrode surface during the fabrication process. The EIS curve includes a semicircular part and a linear part. The semicircular part at higher frequencies corresponds to the electron-transfer-limited process and its diameter is equal to the electron transfer resistance (R_{et}), which controls the electron transfer kinetics of the redox probe at the electrode interface. Meanwhile, the linear part at lower frequencies corresponds to the diffusion process. Figure 3 displays the EIS of bare (a), urchin-like Hi-Ns-TiO_2-coated (b), and monodisperse Np-TiO_2-coated GC electrodes in 2.0 mmol/L $K_3[Fe(CN)_6]/K_4[Fe(CN)_6]$ (1:1) with 0.1 mol/L KCl. For the bare GC electrode, the EIS curve consists of only a linear part, which indicates a diffusion-controlled redox process at the electrode where no substance blocks electron transfer between probe ions and the electrode. In the case of Hi-Ns-TiO_2- and Np-TiO_2-coated electrodes, both curves consist of a semicircular part and a linear part, and the diameter of the semicircle is much less for the former than for the latter. Hence, in both cases the nanostructured TiO_2 coating blocks the electrochemical reaction on the electrode surface due to the electrostatic repulsion between the negatively charged redox couple ions and the negatively charged nanostructured TiO_2 (which has an isoelectric point pI = 5.8). However, the urchin-like Hi-Ns-TiO_2 coating has an interfacial electron transfer resistance (840 Ω) which is

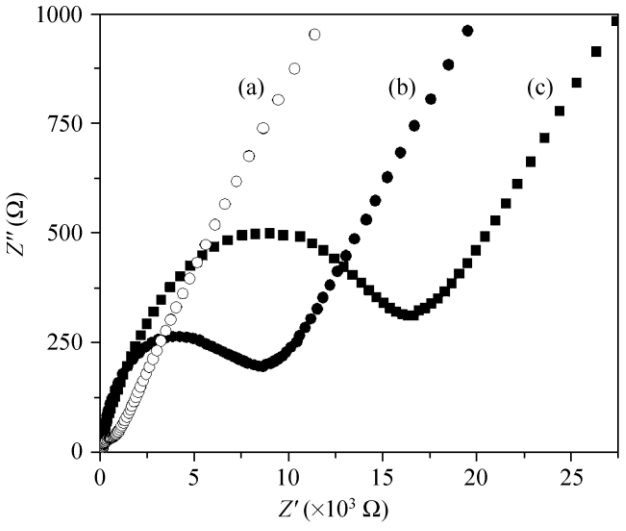

Figure 3 Nyquist plots for bare (a), urchin-like Hi-Ns-TiO_2-coated (b) and monodisperse Np-TiO_2-coated (c) GC electrodes in 2.0×10^{-3} mol/L $K_3[Fe(CN)_6]/K_4[Fe(CN)_6]$ (1:1) with 0.1 mol/L KCl

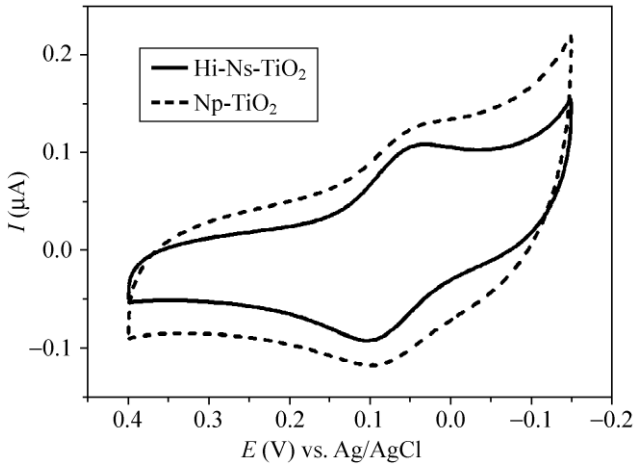

Figure 4 Cyclic voltammograms of 0.56 mg/mL cyt *c* in 25 mmol/L PBS (pH 6.8) at the urchin-like Hi-Ns-TiO_2-coated (solid line) and the monodispersed Np-TiO_2-coated (dashed line) electrodes. Scan rate: 5 mV/s

much lower than that of the Np-TiO_2 coating (1760 Ω). This can be explained in two ways. On the one hand, the urchin-like microstructures result in the formation of two 3-D networks, one consisting of the urchin-like TiO_2 nanowires and the other consisting of the interconnected nanopores, while the latter is also blended with the macropores of the nanosphere coating. Such a nanostructure provides a larger contact area between sensing materials and sensed species than that for the nonhierarchical nanoparticles. On the other hand, due to the ultrathin structure of the nanowires, the charge distribution on the surface of the urchin-like Hi-Ns-TiO_2 may lead to less resistance to the diffusion of probe ions onto the electrode surface than observed with the monodisperse Np-TiO_2. Thus, the Hi-Ns-TiO_2 coating can more effectively promote the transportation and accessibility of target molecules and facilitate the transfer of electrons, which is the key to its much enhanced sensitivity and reduced nonfaradaic behavior.

3.3 Direct electrochemistry of cyt *c* at Hi-Ns-TiO_2-coated and Np-TiO_2-coated electrodes

3.3.1 Comparison of the two coated electrodes in response to a given concentration of cyt c

Figure 4 depicts cyclic voltammograms (CVs) of 0.56 mg/mL cyt *c* in 25 mmol/L PBS (pH 6.8) on Hi-Ns-TiO_2- and Np-TiO_2-coated electrodes at a scan rate of 5 mV/s. A pair of well-defined redox peaks were observed on the Hi-Ns-TiO_2-coated electrode at $E_{pc} = 0.033$ V, $E_{pa} = 0.103$ V, with a separation of 70 mV, which can be attributed to the quasi-reversible redox process of the heme group of cyt *c*. The formal potential was 0.068 V, and the cathodic and anodic peak currents were nearly equal to each other, which is in good agreement with the reported characteristics of a native cyt *c* [26–28]. In contrast, a pair of rather ill-defined peaks with a lower faradaic current (~74%) and a high capacitance current was obtained on the Np-TiO_2-coated electrode in the same solution. This suggests better reversibility of the direct electrochemistry of cyt *c* at the Hi-Ns-TiO_2 electrode.

Cyt *c* consists of a single polypeptide and a heme. In the native conformation, the heme moiety is covalently bound by two thioether bridges to two cysteine residues (Cys14 and Cys17) and axially ligated with histidine (His18) and methionine (Met80) residues [29]. To form these bonds, the heme is embedded in the hydrophobic interior of the globular polypeptide, leaving an edge exposed to solvent. The electron transfer of cyt *c* is believed to occur at the edge of the heme [30]. In living cells, excess positive charge, in the form of lysine residues surrounding the exposed heme edge of cyt *c*, allows it to complex and transfer electrons with protein partners that display anionic surface domains [31]. In the presence of Np-TiO_2 on

the electrode surface, the negatively charged Np-TiO_2 could interact with the positively charged lysine residues of cyt *c* to force it into an appropriate orientation for electron transfer through bringing the heme group closer to the electrode surface and preventing the denaturing adsorption, leading to the redox response of cyt *c* (the dashed line in Fig. 4). The Hi-Ns-TiO_2-coated electrode exhibited better electrochemical reversibility (the solid line in Fig. 4), which can be ascribed to the advantages offered by both the hierarchical architecture of the TiO_2 nanospheres and the ultrathin size and single-crystalline nature of the nanowires. Firstly, higher efficiency of transportation and adsorption of cyt *c* can be obtained on the Hi-Ns-TiO_2 electrode due to high specific surface area of the urchin-like nanospheres, the ordered spatial orientation and arrangement of nanowires, and the good biocompatibility of the single-crystalline nanowires. Secondly, the ultrathin nanowires may be suitable in size for electrostatic interaction with cyt *c*. Excellent biocompatibility associated with quantum size effects and outstanding structural stability associated with the hierarchical nanoarchitecture, results in cyt *c* being more effectively orientated and aligned in a more ordered way on the ultrathin nanowires in the hierarchical structure required for rapid electron transfer; this is crucial in ensuring the reversible, sensitive and stable response of cyt *c* at the Hi-Ns-TiO_2-coated electrode. Thirdly, the lower electron transfer resistance of Hi-Ns-TiO_2 electrode (as shown by the EIS data) and the reduced electrode fouling by the protein (as a result of the appropriate orientation of cyt *c*) contribute to the lower capacitance current [32]. Thus, the Hi-Ns-TiO_2 electrode exhibited better reversibility for direct electrochemistry of cyt *c* than the Np-TiO_2 electrode.

3.3.2 *Sensitivity and stability of the two coated electrodes*

Figure 5 shows the voltammetric detection of cyt *c* for a series of concentrations in 25 mmol/L PBS (pH 6.8) at the Hi-Ns-TiO_2-coated electrode. The redox peak potential occurred at *ca.* 0.068 V. The peak current (I_P) increased linearly as the cyt *c* concentration (*c*) increased in the range 0.16 to 2 mg/mL, using the calibration plot method (Fig. 6(a)) with a correlation coefficient of 0.9989. The linear regression equation is expressed as $I = 35.56 + 53.18\ c$ (I in nA; c in mg/mL). At the Np-TiO_2-coated electrode, the peak current was much less than for the Hi-Ns-TiO_2-coated electrode. As shown in Fig. 6(b), its linear regression equation is expressed as $I = 26.55 + 39.54\ c$ (I in nA; c in mg/mL). The Hi-Ns-TiO_2 electrode exhibited higher sensitivity for detection of cyt *c* than the Np-TiO_2 electrode. In addition, the Hi-Ns-TiO_2-coated electrode also exhibited good stability in response to cyt *c*. Here, both operational and storage stability were measured, since these are important for practical application of an electrode. When the coated electrode was scanned

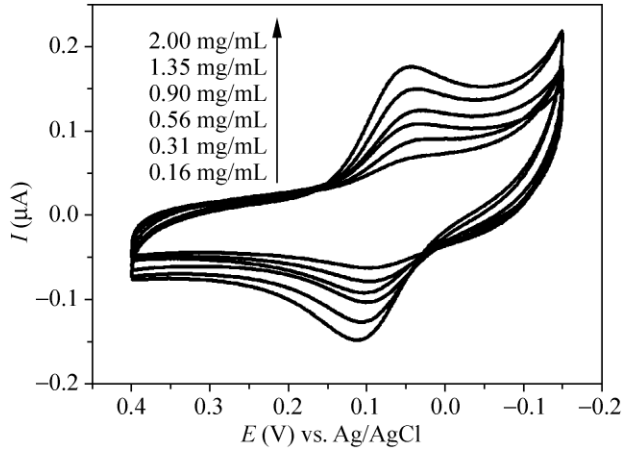

Figure 5 Cyclic voltammograms for a series of concentrations of cyt *c* in 25 mmol/L PBS (pH 6.8) at the Hi-Ns-TiO_2-coated electrode. Scan rate: 5 mV/s

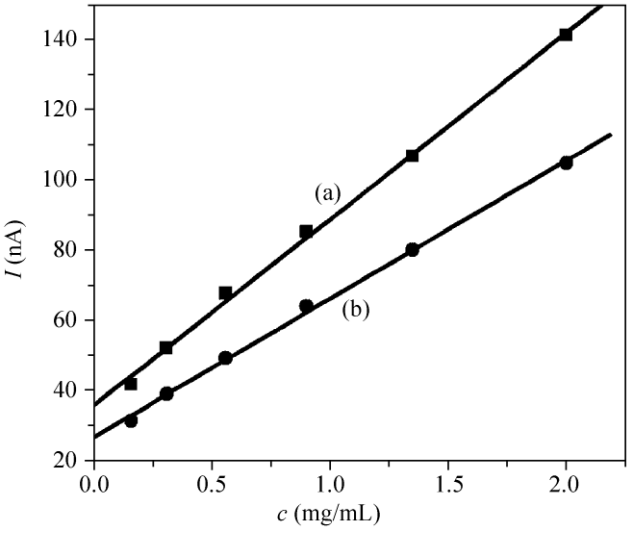

Figure 6 Plots of cathodic peak current vs. cyt *c* concentration at the Hi-Ns-TiO_2-coated (a) and the monodisperse Np-TiO_2-coated (b) electrodes

consecutively with a certain concentration of cyt *c*, the response current gradually increased over several initial cycles. Once equilibrated, the coated electrode yielded reproducible redox signals, until the surrounding conditions were changed. The storage stability was examined during a period of 20 days with intermittent measurements every two days. When not in use, the coated electrode was stored in PBS. The response of the electrode was maintained at about 95% of the initial values. The high sensitivity and good stability are attributed to quantum size effects, and the hierarchical nanostructure, excellent structural stability and suitable biocompatibility of the urchin-like TiO_2 nanospheres, which makes the Hi-Ns-TiO_2 electrode a potential practical sensor for cyt *c*.

3.3.3 *Kinetics of the heterogeneous electron transfer*

Figure 7 shows the voltammetric response to 1.35 mg/mL cyt *c* in 25 mmol/L PBS (pH 6.8) at the Hi-Ns-TiO_2-coated electrode with various scan rates. In the range 1–100 mV/s, the cathodic peak current was found to be proportional to the square root of the scan rates, which corresponds to a diffusion controlled process [33]. From the increase in ΔE_p with the scan rate, the heterogeneous electron transfer rate constant (k_0) can be calculated to be 1.44×10^{-3} cm/s according to the Nicholson equation [34]. The redox process at the Np-TiO_2 electrode was also found to be diffusion-controlled with the value of k_0 calculated to be 1.17×10^{-3} cm/s. Based on these results, the Hi-Ns-TiO_2 electrode is more suitable to model the protein partners for further investigation of cyt *c* than the Np-TiO_2 electrode.

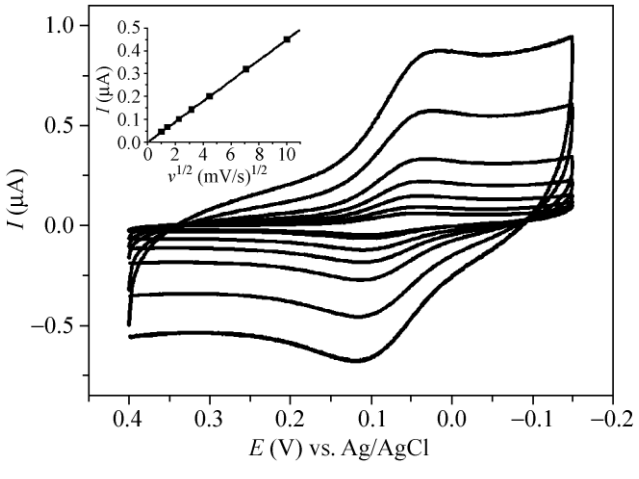

Figure 7 Cyclic voltammograms of 1.35 mg/mL cyt *c* in 25 mmol/L PBS (pH 6.8) at the Hi-Ns-TiO_2-coated electrode with various scan rates: 1 mV/s, 2 mV/s, 5 mV/s, 10 mV/s, 20 mV/s, 50 mV/s, 100 mV/s. Inset: Plot of cathodic peak current vs. the square root of scan rate

3.4 Direct electrochemistry of cyt *c* within the low concentration range

An interesting electrochemical phenomenon was observed at the Hi-Ns-TiO_2-coated electrode in 25 mmol/L PBS (pH 6.8) containing cyt *c* at a concentration lower than 0.16 mg/mL, as shown in Fig. 8. At a concentration of 0.11 mg/mL, a pair of shoulder peaks started to appear at *ca.* 0.18 and 0.28 V with the formal potential of *ca.* 0.23 V, while the couple at *ca.* 0.068 V became weaker. At 0.05 mg/mL, the couple at *ca.* 0.23 V grew slightly stronger and the couple at *ca.* 0.068 V became much weaker. The separation between the formal potentials for the two couples is more than 200 mV, and thus the two redox processes correspond to two species both related to cyt *c*. The characteristics of the redox process at *ca.* 0.23 V are: (1) the Fe^{III} to Fe^{II} reduction of cyt *c* became easier but the re-oxidation became more difficult compared with the process at *ca.* 0.068 V, where cyt *c* is in the native conformation; (2) the peak separation increased to 100 mV compared with 70 mV for the native cyt *c* at a scan rate of 5 mV/s. Based on these observations, the new species may be ascribed to a partially unfolded cyt *c* [35]. Its

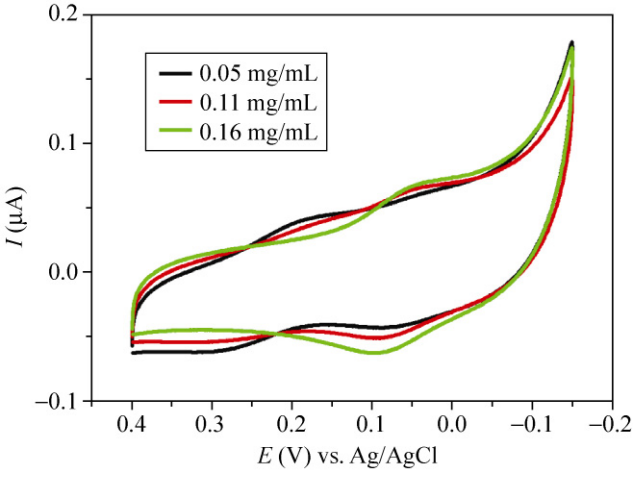

Figure 8 Cyclic voltammograms of low concentrations of cyt *c* in 25 mmol/L PBS (pH 6.8) at the Hi-Ns-TiO_2-coated electrode: 0.05 mg/mL, 0.11 mg/mL, 0.16 mg/mL. Scan rate: 5 mV/s

formation is directly related to a high relative ionic strength (high I/c).

The UV–vis spectra in Fig. 9 shows two obvious peaks located at 408 and 508 nm for all the above three solutions with different concentrations of cyt *c*, corresponding to the Soret band and Q-band of native cyt *c*, respectively. This suggests that high values of I/c did not induce a conformational change of cyt *c* in 25 mmol/L PBS (pH 6.8). Circular dichroism spectra have also demonstrated that no conformational change was detected in cyt *c* in a buffer solution with high or low ionic strength [36, 37]. Thus, it can be deduced that partially unfolded cyt *c* was formed on the Hi-Ns-TiO_2 electrode surface, induced by the high relative ionic strength. As the concentration of cyt *c* in 25 mmol/L PBS (pH 6.8) decreased (I/c increased), the net positive charges on the surface of cyt *c* slightly decreased as a result of specific ion binding. When the surface charges decreased to a limiting state (on going from a cyt *c* concentration of 0.16 to 0.11 mg/mL), a minor conformational destabilization of cyt *c* could occur in order to reach dynamic equilibrium between the protein and the electrolyte. When such a cyt *c* species reached the Hi-Ns-TiO_2 electrode, the destabilization induced the partial unfolding of cyt *c* with the help of Hi-Ns-TiO_2, leading to the redox response at *ca.* 0.23 V. At a concentration of 0.05 mg/mL cyt *c*, the greater destabilization caused more cyt *c* molecules to partially unfold on the Hi-Ns-TiO_2 electrode, leading to larger redox response at *ca.* 0.23 V. Thus, in 25 mmol/L PBS (pH 6.8), the high value of I/c together with the properties of the Hi-Ns-TiO_2 both contributed to the partial unfolding of cyt *c* on electrode.

The effect of the state of Hi-Ns-TiO_2 on the conformation of cyt *c* was also investigated. Figure 10 shows eight and three consecutive cyclic scans of freshly prepared Hi-Ns-TiO_2 (PBS) and Hi-Ns-TiO_2 electrodes in 0.05 mg/mL cyt *c* in PBS (25 mmol/L, pH 6.8). The Hi-Ns-TiO_2 (PBS) electrode exhibited a similar response to partial unfolding cyt *c*, but a stronger response to native cyt *c* than the Hi-Ns-TiO_2 electrode, when both electrodes reached a steady state in 0.05 mg/mL cyt *c* in PBS (25 mmol/L, pH 6.8). It should be noted that the Hi-Ns-TiO_2 (PBS)-coated electrode may take on more negative charges because PBS was used as dispersant in the preparation of the electrode. In 0.05 mg/mL cyt *c* in PBS (25 mmol/L, pH 6.8), cyt *c* with medium or slightly higher positive charge is more sensitive to the negative charges on the electrode surface relative to cyt *c* with lower positive charges. Thus, more cyt *c* molecules orientated in the native form on the Hi-Ns-TiO_2 (PBS) electrode than on the Hi-Ns-TiO_2 electrode, leading to larger current at *ca.* 0.068 V. This suggests that the state of charge on the Hi-Ns-TiO_2 surface plays an important role in the direct electrochemistry of cyt *c*. In addition, electrodes coated with the Np-TiO_2, Au nanoparticles or Si nanowires were also found to exhibit a new pair of redox

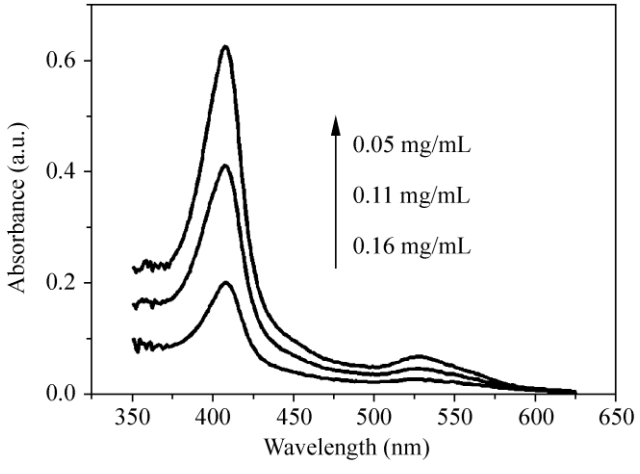

Figure 9 UV–vis spectra of 0.05 mg/mL, 0.11 mg/mL, and 0.16 mg/mL cyt *c* in 25 mmol/L PBS (pH 6.8)

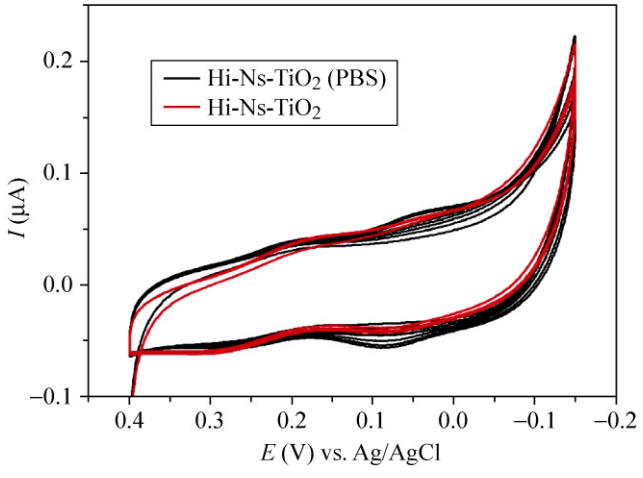

Figure 10 Eight and three consecutive cyclic potential scans of two freshly prepared electrodes formed by deposition of Hi-Ns-TiO_2 from PBS (black line) and EtOH (red line) in 0.05 mg/mL cyt *c* PBS (25 mmol/L, pH 6.8)

peaks at *ca*. 0.23 V in response to 0.05 mg/mL cyt *c* in 25 mmol/L PBS (pH 6.8) (data not shown). Nevertheless, the Hi-Ns-TiO_2-coated electrode had a better response to cyt *c* at this potential due to the quantum size effect and its excellent structural stability. Further studies are under way to fully understand the effect of relative ionic strength (*I*/*c*) on the conformational change of cyt *c* on an electrode. However, it can be concluded that in 25 mmol/L PBS (pH 6.8), the distribution of the surface charges of cyt *c* is crucial in determining the orientation and conformation of cyt *c* on an electrode, and the state of an electrode surface also has a significant effect on the orientation and conformation.

4. Conclusions

Urchin-like TiO_2 nanospheres hierarchically assembled with ultrathin quantum nanowires have been synthesized by a novel wet chemical method. A hierarchically nanostructured quantum TiO_2 electrode exhibited better reversibility for the direct electrochemistry of cyt *c* and higher sensitivity for the detection of cyt *c* in comparison with a monodisperse Np-TiO_2 electrode. The excellent performance is attributed to the ultrathin structure of the nanowires, the more ordered spatial orientation and arrangement of the nanowires, and the excellent structural stability as well as good biocompatibility of the hierarchical TiO_2 nanospheres. Relative ionic strength had significant effect on the direct electrochemistry. In 25 mmol/L PBS (pH 6.8), the distribution of surface charges on cyt *c* induced by changing the *I*/*c* ratio has a decisive effect on the orientation and conformation of cyt *c* on an electrode (whether it adopts a native conformation or a partially unfolded one), and the state of the electrode surface also plays an important role in determining the orientation and conformation. The results provide new insight into our understanding of biological processes involving cyt *c*.

Acknowledgements

This work was supported by the National Basic Research Program of China (No. 2010CB934700) and the National Natural Science Foundation of China (Nos. 20973019, 50902007, and 50725208).

References

[1] Chen, H. J.; Wang, Y. L.; Dong, S. J.; Wang, E. K. Direct electrochemistry of cytochrome *c* at gold electrode modified with fumed silica. *Electroanalysis* **2005**, *17*, 1801–1805.

[2] Stoll, C.; Kudera, S.; Parak, W. J.; Lisdat, F. Quantum dots on gold: Electrodes for photoswitchable cytochrome *c* electrochemistry. *Small* **2006**, *2*, 741–743.

[3] Feng, J. J.; Xu, J. J.; Chen, H. Y. Direct electron transfer and electrocatalysis of hemoglobin adsorbed onto electrodeposited mesoporous tungsten oxide. *Electrochem. Comm.* **2006**, *8*, 77–82.

[4] Rezaei-Zarchi, S.; Saboury, A. A.; Javed, A. Electrochemical study of horseradish peroxidase using the nanosilver-modified graphite electrode and its application to hydrogen peroxide biosensor. *J. New Mat. Electrochem. Systems* **2008**, *11*, 199–203.

[5] Ni, X. M.; Zhao, Q. B.; Zhang, Y. F.; Song, J. M.; Zheng, H. G.; Yang, K. Large scale synthesis and electrochemical characterization of hierarchical β-$Ni(OH)_2$ flowers. *Solid State Sci.* **2006**, *8*, 1312–1317.

[6] Wang, H. E.; Qian, D.; Lu, Z. G.; Li, Y. K.; Cheng, R. J.; Li, Y. J. Facile synthesis and electrochemical properties of hierarchical MnO_2 submicrospheres and $LiMn_2O_4$ microspheres. *J. Phys. Chem. Solids* **2007**, *68*, 1422–1427.

[7] Zhang, Y.; Chen, Y. G.; Liu, H.; Zhou, Y. Q.; Li, R. Y.; Cai, M.; Sun, X. L. Three-dimensional hierarchical structure of single crystalline tungsten oxide nanowires: Construction, phase transition, and voltammetric behavior. *J. Phys. Chem. C* **2009**, *113*, 1746–1750.

[8] Wang, H. B.; Pan, Q. M.; Cheng, Y. X.; Zhao, J. W.; Yin, G. P. Evaluation of ZnO nanorod arrays with dandelion-like morphology as negative electrodes for lithium-ion batteries. *Electrochim. Acta* **2009**, *54*, 2851–2855.

[9] Geng, Y.; Wang, X. L.; Chen, W.; Cai, Q.; Nan, C. W.; Li, H. D. Synthesis, characterization and application of novel bicontinuous mesoporous silica with hierarchical pore structure. *Mater. Chem. Phys.* **2009**, *116*, 254–260.

[10] Ren, H. X.; Huang, X. J.; Yarimaga, O.; Choi, Y. K.; Gu, N. A cauliflower-like gold structure for superhydrophobicity. *J. Coll. Interf. Sci.* **2009**, *334*, 103–107.

[11] Jiang, L. Y.; Wu, X. L.; Guo, Y. G.; Wan, L. J. SnO_2-based hierarchical nanomicrostructures: Facile synthesis and their

applications in gas sensors and lithium-ion batteries. *J. Phys. Chem. C* **2009**, *113*, 14213–14219.

[12] Ren, H. X.; Huang, X. J.; Kim, J. H.; Choi, Y. K.; Gu, N. Pt/Au bimetallic hierarchical structure with micro/nano-array via photolithography and electrochemical synthesis: From design to GOT and GPT biosensors. *Talanta* **2009**, *78,* 1371–1377.

[13] Song, M. J.; Hwang, S. W.; Whang, D. Amperometric glucose biosensor based on a Pt-dispersed hierarchically porous electrode. *J. Korean Phys. Soc.* **2009**, *54*, 1612–1618.

[14] Cuendet, P.; Grätzel, M. Light-induced reduction of cytochrome *c* by colloidal TiO_2. *Bioelectrochem. Bioenerg.* **1986**, *16*, 125–133.

[15] McKenzie, K. J.; Marken, F.; Opallo, M. TiO_2 phytate films as hosts and conduits for cytochrome *c* electrochemistry. *Bioelectrochemistry* **2005**, *66*, 41–47.

[16] Cao, H. M.; Zhu, Y. H.; Tang, L. H.; Yang, X. L.; Li, C. Z. A glucose biosensor based on immobilization of glucose oxidase into 3D macroporous TiO_2. *Electroanalysis* **2008**, *20*, 2223–2228.

[17] Topoglidis, E.; Lutz, T.; Durrant, J. R.; Palomares, E. Interfacial electron transfer on cytochrome-*c* sensitised conformally coated mesoporous TiO_2 films. *Bioelectrochemistry* **2008**, *74*, 142–148.

[18] Zhang, Y.; He, P. L.; Hu, N. F. Horseradish peroxidase immobilized in TiO_2 nanoparticle films on pyrolytic graphite electrodes: Direct electrochemistry and bioelectrocatalysis. *Electrochim. Acta* **2004**, *49*, 1981–1988.

[19] Wen, Z. H.; Ci, S. Q.; Li, J. H. Pt nanoparticles inserting in carbon nanotube arrays: Nanocomposites for glucose biosensors. *J. Phys. Chem. C* **2009**, *113*, 13482–13487.

[20] Zhang, L.; Zhang, Q.; Li, J. H. Layered titanate nano-sheets intercalated with myoglobin for direct electrochemistry. *Adv. Funct. Mater.* **2007**, *17*, 1958–1965.

[21] Cao, X.; Wang, N.; Li, L. D.; Guo, L. Synthesis and characterization of waxberry-like microstructures ZnO for biosensors. *Sens. Actuators B* **2008**, *129*, 268–273.

[22] Li, Y.; Sasaki, T.; Shimizu, Y.; Koshizaki, N. Hexagonal-close-packed, hierarchical amorphous TiO_2 nanocolumn arrays: Transferability, enhanced photocatalytic activity, and superamphiphilicity without UV irradiation. *J. Am. Chem. Soc.* **2008**, *130*, 14755–14762.

[23] Gong, J.; Yao, P.; Duan, H. W.; Gu, S. H.; Chunyu, L. J. Structural transformation of cytochrome *c* and apo cytochrome *c* induced by sulfonated polystyrene. *Biomacromolecules* **2003**, *4*, 1293–1300.

[24] Koppenol, W. F.; Margoliash, E. The asymmetric distribution of charges on the surface of horse cytochrome *c*. Functional implications. *J. Biol. Chem.* **1982**, *257*, 4426–4437.

[25] Moore, G. R.; Eley, C. G. S.; Williams, G. Electron transfer reactions of class I cytochromes *c*. In *Advances in Inorganic and Bioinorganic Mechanisms*. Sykes, A. G., Ed.; Academic Press: New York, 1984; Vol. 3, pp. 1–96.

[26] Armstrong, F. A.; Cox, P. A.; Hill, H. A. O.; Lowe, V. J.; Oliver, B. N. Metal ions and complexes as modulators of protein-interfacial electron transport at graphite electrodes. *J. Electroanal. Chem.* **1987**, *217*, 331–366.

[27] Brown, K. R.; Fox, A. P.; Natan, M. J. Morphology-dependent electrochemistry of cytochrome *c* at Au colloid-modified SnO_2 electrodes. *J. Am. Chem. Soc.* **1996**, *118*, 1154–1157.

[28] Wang, J. X.; Li, M. X.; Shi, Z. J.; Li, N. Q.; Gu, Z N. Direct electrochemistry of cytochrome *c* at a glassy carbon electrode modified with single-wall carbon nanotubes. *Anal. Chem.* **2002**, *74*, 1993–1997.

[29] George, P.; Lyster, R. L. J. Crevice structures in hemoprotein reactions. *Proc. Natl. Acad. Sci. USA* **1958**, *44*, 1013–1029.

[30] Moore, G. R.; Huang, Z. X.; Eley, C. G. S.; Barker, H. A.; Williams, G.; Robinson, M. N.; Williams, R. J. P. Electron transfer in biology. The function of cytochrome *c*. *Faraday Discuss. Chem. Soc.* **1982**, *74*, 311–329.

[31] Ferguson-Miller, S.; Brautigan, D. L.; Margoliash, E. Kinetics of reaction of carboxydinitrophenyl cytochromes *c* with cytochrome *c* oxidase. *J. Biol. Chem.* **1978**, *253*, 149–159.

[32] Szücs, Á.; Noák, M. Stable and reversible electrochemistry of cytochrome *c* on bare electrodes. Part 1. Effect of ionic strength. *J. Electroanal. Chem.* **1995**, *383*, 75–84.

[33] Mu, C.; Yu, Y. X.; Liao, W.; Zhao, X. S.; Xu, D. S.; Chen, X. H.; Yu, D. P. Silicon nanotube array/gold electrode for direct electrochemistry of cytochrome *c*. *J. Phys. Chem. B* **2007**, *111*, 1491–1495.

[34] Nicholson, R. S. Theory and application of cyclic voltammetry for measurement of electrode reaction kinetics. *Anal. Chem.* **1965**, *37*, 1351–1355.

[35] Moghaddam, A. B.; Ganjali, M. R.; Dinarvand, R.; Razavi, T.; Saboury, A. A.; Moosavi-Movahedi, A. A.; Norouzi, P. Direct electrochemistry of cytochrome *c* on electrodeposited nickel oxide nanoparticles. *J. Electroanal. Chem.* **2008**, *614*, 83–92.

[36] Daido, T.; Akaike, T. Electrochemistry of cytochrome *c*: Influence of coulombic attraction with indium tin oxide electrode. *J. Electroanal. Chem.*, **1993**, *344*, 91–106.

[37] Zhou, J. H.; Lu, X. B.; Hu, J. Q.; Li, J. H. Reversible immobilization and direct electron transfer of cytochrome *c* on pH sensitive polymer interface. *Chem. Eur. J.*, **2007**, *13*, 2847–2853.